J|A|C|S
ARTICLES

Published on Web 11/10/2009

Unusual Bonding in Trisilaallene and Related Heavy Allenes

Mitsuo Kira,*,† Takeaki Iwamoto,*,‡ Shintaro Ishida,† Hidenori Masuda,†
Takashi Abe,† and Chizuko Kabuto‡

Department of Chemistry, and Research and Analytical Center for Giant Molecules, Graduate School of Science, Tohoku University, Aoba-ku, Sendai, 980-8578, Japan

Received June 5, 2009; E-mail: mkira@mail.tains.tohoku.ac.jp (M.K.); iwamoto@m.tains.tohoku.ac.jp (T.I.)

Abstract: The synthesis, X-ray and spectroscopic analysis, and unusual bonding and structure among heavy group-14 element congeners of allene (heavy allenes) [$R_2M{=}M'{=}MR_2$; M = M′ = Si (**1a**), M = Si, M′ = Ge (**1b**), M = Ge, M′ = Si (**1c**), and M = M′ = Ge (**1d**)] are comparatively discussed. Using DFT calculations and PMO theory, the origin of the bent and fluxional skeleton of the heavy allenes is ascribed to the Jahn−Teller distortion associated with the effective $\pi-\sigma^*$ mixing ($\pi-\sigma^*$ distortion). This type of distortion is suggested to be a key concept for qualitative description of the unusual bonding of unsaturated compounds of heavy main-group elements.

Introduction

Recent advances in the chemistry of unsaturated compounds of silicon and heavier group-14 elements[1,2] have revealed that their bonding and structure are often remarkably different from those of the corresponding carbon compounds in which s/p-hybridization models are valid. For example, theoretical studies have shown that geometry of heavy ethylenes ($H_2M{=}MH_2$, M = Si, Ge, and Sn) and heavy acetylenes (HM≡MH) is trans-bent in contrast to planar ethylene ($H_2C{=}CH_2$) and linear acetylene (HC≡CH), that heavy methyl radicals ($H_3M^{\bullet}$) are pyramidal, while methyl radical ($H_3C^{\bullet}$) is planar, and that the ground state of heavy methylenes (H_2M:) is singlet with a narrow bond angle, while that of methylene (H_2C:) is triplet with a wide bond angle.[2] The structural difference between carbon compounds and their heavier group-14 element congeners has been evidenced also by many experimental studies.[1] The origin of the unusual bonding and structure of heavy group-14 unsaturated molecules has been explained individually in various ways including the double-dative bond model,[3] Jahn−Teller distortion,[2c,4] and Carter−Goddard−Mauliu−Trinquire (CGMT) models[5,6] for trans-bent heavy ethylenes.

Chart 1

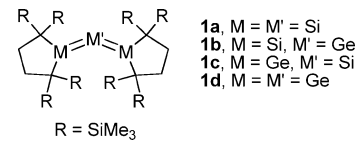

1a, M = M' = Si
1b, M = Si, M' = Ge
1c, M = Ge, M' = Si
1d, M = M' = Ge

We have reported recently the synthesis of a series of $R_2M{=}M'{=}MR_2$ type stable heavy allenes **1a**−**1d** (Chart 1) and their quite unusual bonding properties.[7] In contrast to normal carbon allenes that have a rigid linear C−C−C skeleton and two orthogonal C−C π bonds, the heavy allenes have particularly the following characteristics: (1) the geometries of all the

† Department of Chemistry.
‡ Research and Analytical Center for Giant Molecules.

(1) For recent reviews of unsaturated bonds to heavier group-14 elements, see: (a) Okazaki, R.; West, R. *Adv. Organomet. Chem.* **1996**, *39*, 231. (b) Weidenbruch, M. In *The Chemistry of Organic Silicon Compounds*; Rappoport, Z., Apeloig, Y., Eds.; John Wiley & Sons: Chichester, U.K., 2001; Vol. 3, p 391. (c) West, R. *Polyhedron* **2002**, *21*, 467. (d) Kira, M.; Iwamoto, T. *J. Organomet. Chem.* **2000**, *611*, 236. (e) Kira, M.; Iwamoto, T.; Ishida, S. In *Organosilicon Chemistry VI—From Molecules to Materials*; Auner, N., Weis, J., Eds.; Wiley-VCH: Weinheim, 2005; p 25. (f) Kira, M. *J. Organomet. Chem.* **2004**, *689*, 4475. (g) Kira, M.; Iwamoto, T. *Adv. Organomet. Chem.* **2006**, *54*, 73. (h) Power, P. P. *Chem. Rev.* **1999**, *99*, 3463. (i) Power, P. P. *Chem. Commun.* **2003**, 2091. (j) Power, P. P. *Organometallics* **2007**, *26*, 4362. (k) Sekiguchi, A.; Ichinohe, M.; Kinjo, R. *Bull. Chem. Soc. Jpn.* **2006**, *79*, 825. (l) Lee, V. Y.; Sekiguchi, A. *Angew. Chem., Int. Ed.* **2007**, *46*, 6596. (m) Tsumuraya, T.; Batcheller, S. A.; Masamune, S. *Angew. Chem., Int. Ed. Engl.* **1991**, *30*, 902. (n) Weidenbruch, M. *J. Organomet. Chem.* **2002**, *646*, 39.

(2) For reviews of theoretical aspects of unsaturated bonds to heavier group-14 elements, see: (a) Apeloig, Y. In *The Chemistry of Organic Silicon Compounds*; Patai, S., Rappoport, Z., Eds.; John Wiley & Sons: Chichester, U.K., 1989; Vol. 1, p 57. (b) Karni, M.; Kapp, J.; Schleyer, P. v. R.; Apeloig, Y. In *The Chemistry of Organic Silicon Compounds*; Rappoport, Z., Apeloig, Y., Eds.; John Wiley & Sons: Chichester, U.K., 2001; Vol. 3, p 1. (c) Grev, R. S. *Adv. Organomet. Chem.* **1991**, *33*, 125. (d) Mackay, K. M. In *The Chemistry of Organic Silicon Compounds*; Patai, S., Ed.; John Wiley & Sons: Chichester, U.K., 1995; p 97. (e) Scheldrick, W. S. In *The Chemistry of Organic Silicon Compounds*; Patai, S., Rappoport, Z., Eds.; John Wiley & Sons: Chichester, U.K., 1989; Vol. 1, p 227.

(3) (a) Davidson, P. J.; Harris, D. H.; Lappert, M. F. *J. Chem. Soc., Dalton Trans.* **1976**, 2268. (b) Trinquier, G.; Malrieu, J. P.; Riviere, P. *J. Am. Chem. Soc.* **1982**, *104*, 4529.

(4) (a) Goldberg, D. E.; Hitchcock, P. B.; Lappert, M. F.; Thomas, K. M.; Thorne, A. J.; Fjeldberg, T.; Haaland, A.; Schilling, B. E. R. *J. Chem. Soc., Dalton Trans.* **1986**, 2387. (b) Jacobsen, H.; Ziegler, T. *J. Am. Chem. Soc.* **1994**, *116*, 3667.

(5) (a) Trinquier, G.; Malrieu, J. P. *J. Am. Chem. Soc.* **1987**, *109*, 5303. (b) Malrieu, J. P.; Trinquier, G. *J. Am. Chem. Soc.* **1989**, *111*, 5916. (c) Trinquier, G.; Malrieu, J. P. *J. Phys. Chem.* **1990**, *94*, 6184.

(6) (a) Driess, M.; Grützmacher, H. *Angew. Chem., Int. Ed. Engl.* **1996**, *36*, 828. (b) Carter, E. A.; Goddard, W. A., III. *J. Phys. Chem.* **1986**, *90*, 998. (c) Trinquier, G.; Malrieu, J.-P. In *The Chemistry of Functional Group, Supplement A; The Chemistry of Double-Bonded Functional Group*; Patai, S., Ed.; Wiley: Chichester, U.K., 1989; Vol. 2, Part 1. (d) Trinquier, G. *J. Am. Chem. Soc.* **1990**, *112*, 2130.

(7) (a) Ishida, S.; Iwamoto, T.; Kabuto, C.; Kira, M. *Nature* **2003**, *421*, 725. (b) Iwamoto, T.; Masuda, H.; Kabuto, C.; Kira, M. *Organometallics* **2005**, *24*, 197. (c) Iwamoto, T.; Abe, T.; Kabuto, C.; Kira, M. *Chem. Commun.* **2005**, 5190. (d) Iwamoto, T.; Abe, T.; Ishida, S.; Kabuto, C.; Kira, M. *J. Organomet. Chem.* **2007**, *692*, 263.

synthesized heavy allenes are not linear but bent with the M−M′−M bond angles of 122−137°, (2) the bent M−M′−M skeletons are not rigid but fluxional both in the solid state and in solution, and (3) significant conjugation exists between the two M═M′ double bonds in a heavy allene. In this article, we discuss the synthesis, spectroscopic properties, and unusual bonding and structure of **1a**−**1d**.

Using DFT calculations and perturbation molecular orbital (PMO) theory,[8] the origin of the bent and fluxional skeleton of heavy allenes is ascribed to the Jahn−Teller distortion associated with the effective $\pi-\sigma^*$ mixing (this type of distortion is abbreviated as $\pi-\sigma^*$ distortion in this article). The $\pi-\sigma^*$ distortion that has been also applied to the explanation of nonplanarity of heavy methyl radicals[2b,9] as well as singlet multiplicity of heavy carbenes[10] would be a key concept for qualitative description of the unusual bonding of unsaturated compounds of heavy main-group elements in general because intrinsically they form low-lying σ^* orbitals mixable with π bonding orbitals.

Very recently, Bertrand et al. have synthesized highly strained carbon allenes built in small rings[11] and generated a lively discussion on their unusual electronic structure.[12] Using the PMO theory, the bonding nature of the bent cyclic allenes is compared with that of the bent heavy allenes.

Results and Discussion

Synthesis. Trisilaallene **1a**,[7a] 1,3-digermasilaallene **1c**,[7b] and trigermaallene **1d**[7b] are synthesized by the reactions of silylene **2**[13] and germylene **3**[14] with metal tetrachlorides forming the corresponding tetrachlorodimetallanes **4a**, **4c**, and **4d**[15] followed by the reduction with potassium graphite (KC_8) at low temperatures (Scheme 1). The reduction of tetrachlorodimetallanes having Si−Ge and Ge−Ge bonds like **4c** and **4d** is less satisfactory giving the desired heavy allenes in lower yields than that of **4a**. The reaction of silylene **2** with tetrachlorogermane gives the corresponding insertion product **4b** satisfactorily, but its reduction with KC_8 afforded dichlorosilane **5** in a high yield, instead of the desired 2-germadisilaallene **1b** (Scheme 2).[7c] An alternative method shown in eq 1 is applied to the synthesis of **1b**.[7c] Thus, the reduction of a mixture of silylene **2** and the dioxane complex of

Scheme 1

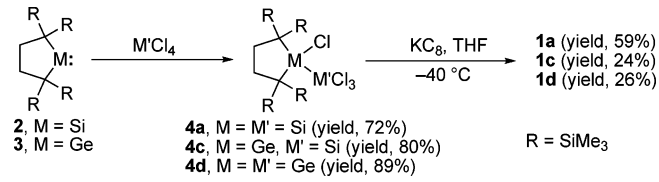

Scheme 2

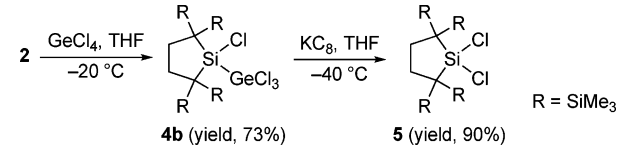

dichlorogermylene with KC_8 gives **1b** in a reasonable yield (eq 1). A similar method is applicable to the synthesis of trigermaallene **1d**.[16]

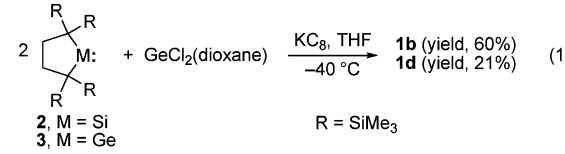

Speculative pathways for the formation of heavy allenes during the reduction of **4a, 4c**, **4d**, and a mixture of **2** (or **3**) and $GeCl_2$ are shown in Scheme 3. Because neither **8** nor **9** has been detected as intermediates during these reactions, the actual reaction pathways seem to be more complicated; in this relation, an attempted substitution of hydrogens to chlorines on the central silicon atom of **10**[15a] that is synthesized by the reaction of **2** with dichlorosilane has failed using various chlorination reagents, CCl_4/benzoyl peroxide, $CCl_4/PdCl_2$, $CuCl_2$/cat. CuI, and $CuCl_2/CH_3CN$ (Scheme 4), probably because substituents on the central silicon are sterically protected effectively by the terminal helmet substituents. Although the cleavage of the M−M′ bond in **4a**, **4c**, and **4d** by KC_8 forming **6** (or **7**) should be accompanied by the formation of $Cl_3M'K$, the fate is not untraced.

X-ray Structures. Molecular structures of heavy allenes **1a**−**1d** have been discussed in detail in previous communications.[7] As discussed later, heavy allenes **1a** and **1b** show remarkable disorder of the central atoms, suggesting dynamic equilibrium among the rotational isomers. The selected structural parameters of the most populated isomers of **1a**−**1d** are compared in Table 1. The M═M′ bond distance is in the order d(Si═Si) < d(Si═Ge) < d(Ge═Ge), which is reasonable because the atomic radius of Ge is larger than that of Si (Si 1.10 Å, Ge 1.25 Å). The M═M′ distances in heavy allenes **1a**−**1d** are comparable or slightly longer than those of known heavy ethylenes but far shorter than the corresponding single bond distances, suggesting the double bond nature of the M−M′ bonds; the typical distances of Si═Si, Si═Ge, and Ge═Ge bonds

(8) (a) Albright, T. A.; Burdett, J. K.; Whangbo, M.-H. *Orbital Interactions in Chemistry*; John Wiley & Sons: New York, 1985. (b) Inagaki, S.; Fujimoto, H.; Fukui, K. *J. Am. Chem. Soc.* **1976**, *98*, 4054.
(9) (a) Levin, C. C. *J. Am. Chem. Soc.* **1975**, *97*, 5649. (b) Bickelhaupt, F. M.; Ziegler, T.; Schleyer, P. v. R. *Organometallics* **1996**, *15*, 1477.
(10) Apeloig, Y.; Pauncz, R.; Karni, M.; West, R.; Steiner, W.; Chapman, D. *Organometallics* **2003**, *22*, 3250, and references cited in.
(11) (a) Lavallo, V.; Dyker, C. A.; Donnadieu, B.; Bertrand, G. *Angew. Chem., Int. Ed.* **2008**, *47*, 5411. (b) Melaimi, M.; Parameswaran, P.; Donnadieu, B.; Frenking, G.; Bertrand, G. *Angew. Chem., Int. Ed.* **2009**, *48*, 4792.
(12) (a) Christl, M.; Engels, B. *Angew. Chem., Int. Ed.* **2009**, *48*, 1538. (b) Lavallo, V.; Dyker, C. A.; Donnadieu, B.; Bertrand, G. *Angew. Chem., Int. Ed.* **2009**, *48*, 1540. (c) Hänninen, M. M.; Peuronen, A.; Tuononen, H. M. *Chem.*—*Eur. J.* **2009**, *15*, 7287.
(13) (a) Kira, M.; Ishida, S.; Iwamoto, T.; Kabuto, C. *J. Am. Chem. Soc.* **1999**, *121*, 9722. For reviews, see: (b) Kira, M.; Iwamoto, T.; Ishida, S. *Bull. Chem. Soc. Jpn.* **2007**, *80*, 258. (c) Kira, M.; Ishida, S.; Iwamoto, T. *Chem. Rec.* **2004**, *4*, 243.
(14) Kira, M.; Ishida, S.; Iwamoto, T.; Ichinohe, M.; Kabuto, C.; Ignatovich, L.; Sakurai, H. *Chem. Lett.* **1999**, 263.
(15) For the insertion of **2** and **3** into different Si−halogen bonds, see: (a) Ishida, S.; Iwamoto, T.; Kabuto, C.; Kira, M. *Silicon Chem.* **2003**, *2*, 137. (b) Uchiyama, K.; Nagendran, S.; Ishida, S.; Iwamoto, T.; Kira, M. *J. Am. Chem. Soc.* **2007**, *129*, 10638. (c) Iwamoto, T.; Kobayashi, M.; Uchiyama, K.; Sasaki, S.; Nagendran, S.; Isobe, H.; Kira, M. *J. Am. Chem. Soc.* **2009**, *131*, 3156.
(16) For the details, see the Supporting Information.
(17) (a) Baines, K. M.; Cooke, J. A. *Organometallics* **1991**, *10*, 3419. (b) Baines, K. M.; Cooke, J. A. *Organometallics* **1992**, *11*, 3487. (c) Lee, V. Ya.; Ichinohe, M.; Sekiguchi, A. *J. Am. Chem. Soc.* **2000**, *122*, 9034. (d) Lee, V. Ya.; Ichinohe, M.; Sekiguchi, A. *J. Am. Chem. Soc.* **2000**, *122*, 12604. (e) Ichinohe, M.; Arai, Y.; Sekiguchi, A.; Takagi, N.; Nagase, S. *Organometallics* **2001**, *20*, 4141. (f) Sekiguchi, A.; Izumi, R.; Ihara, S.; Ichinohe, M.; Lee, V. Ya. *Angew. Chem., Int. Ed.* **2002**, *41*, 1598. (g) Lee, V. Ya.; Sekiguchi, A. *Oraganometallics* **2004**, *23*, 2822.

Scheme 3

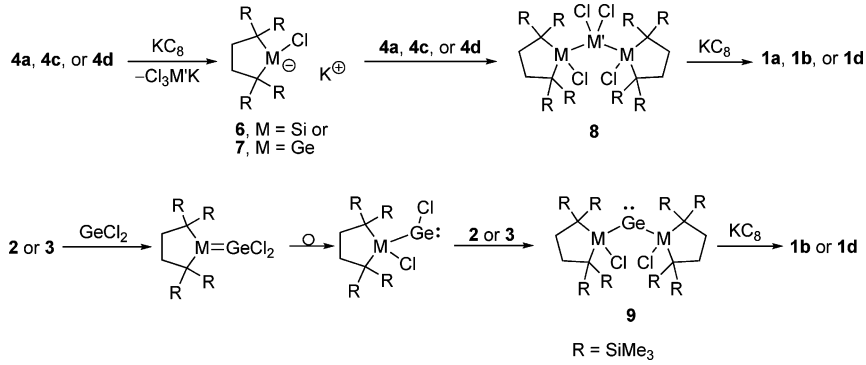

Scheme 4

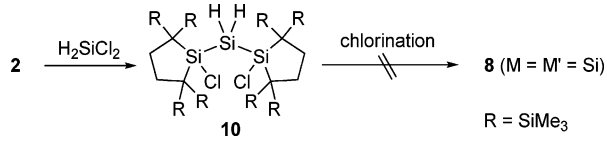

Table 1. Selected Structural Parameters of Heavy Allenes **1a**−**1d**[a]

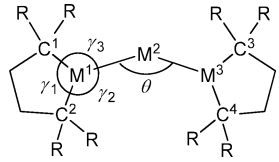

compound	*d*/Å[b]	θ/deg[c]	$\Sigma\gamma_i$@M[d]	disorder[e]
1a	2.183(1) (Si═Si)	136.49(6)	354.5(1)	observed
1b	2.2370(7) (Si═Ge)	132.38(2)	352.51(7)	observed
1c	2.2694(1) (Ge═Si)	125.71(7)	349.3(1)	not observed
1d	2.325(2) (Ge═Ge)	122.61(6)	348.6(2)	not observed

[a] R = $SiMe_3$. Standard deviation is given in parentheses. [b] Average of M^1═M^2 and M^3═M^2 distances. [c] M^1−M^2−M^3 bond angle. [d] Average of the sums of the bond angles around M^1 and M^3. [e] Disorder behavior of M^2 atom.

are known to be in the range of 2.14−2.29,[1g] 2.22−2.25,[17] and 2.21−2.35 Å,[1h,18] respectively, while typical Si−Si, Si−Ge, and Ge−Ge single bond distances are around 2.34, 2.39, and 2.43 Å, respectively.[19] It is interesting to note however that the Si═Ge distance in **1b** with terminal Si atoms is significantly shorter than that of **1c** with terminal Ge atoms, the reason for which remains unknown.

The M−M′−M angles θ of trimetallaallenes decrease in the order **1a** > **1b** > **1c** > **1d**, while a large difference is observed between those of **1b** and **1c**. The sum of the bond angles around terminal atoms ($\Sigma\gamma$@M) that are taken as an index of pyramidalization at the atoms indicates that the pyramidalization at terminal Ge atoms is significantly larger than that at Si atoms as expected.

Dynamic Disorder. Remarkable difference in the disorder behavior was observed between 1,3-disilaallenes **1a** and **1b** and 1,3-digermaallenes **1c** and **1d** in their X-ray structures. The former set shows the disorder, but the latter does not (Table 1). Skeletal geometries ($C^1C^2M^1$═M^2═$M^3C^3C^4$; numbering scheme is shown in Table 1) of **1a**−**1d** obtained by projecting the molecules along the axis through the terminal M^1 and M^3 atoms are shown in Figure 1. X-ray analysis shows that the central atom (M^2) in **1a** (and **1b**) is located at four positions, each in four quadrants A, B, C, and D divided by C^1−M^1−C^2 and C^3−M^3−C^4 planes, while M^2 in **1c** (and **1d**) is observed only in quadrant A. Table 2 shows site occupancy factors (P_A−P_D) of central atom M^2 at various temperatures for **1a** and **1b**. The site occupancy factors are strongly temperature dependent, suggesting the dynamic nature of the disorder.

The temperature dependence of P_A−P_D suggests facile equilibriums among four rotational isomers **1a**^{A}, **1a**^{B}, **1a**^{C}, and **1a**^{D} and among **1b**^{A}, **1b**^{B}, **1b**^{C}, and **1b**^{D}, where **1a**^{X} and **1b**^{X} (X = A−D) are defined as isomers having M^2 in site X of **1a** and **1b**. Plots of $\ln[P_X]$ vs $1/T$ for **1a** and **1b** show good linear relationships as shown in Figure 2. The enthalpies and entropies of **1a**^{X} and **1b**^{X} relative to **1a**^{A} and **1b**^{A}, respectively, are calculated from the linear relationships and listed in Table 2. The enthalpy and entropy differences among the isomers of **1a** and **1b** are very small as expected; the maximum differences of ΔH and ΔS are only 1.14 kcal mol^{-1} and 1.25 cal mol^{-1} K^{-1} for **1a** and 1.44 kcal mol^{-1} and 1.60 cal mol^{-1} K^{-1} for **1b**. It is suggested that the environment is very similar among sites A−D in **1a** and **1b**, though the environmental difference among the sites in **1b** is slightly larger than that in **1a**.

On the other hand, no disorder was observed for **1c** and **1d** between −150 and 0 °C, indicating an isomer with M^2 in site A is more stable than other isomers with ΔG > ca. 2.5 kcal mol^{-1}. The difference in disorder behavior between 1,3-disilaallenes (**1a** and **1b**) and 1,3-digermaallenes (**1c** and **1d**) would be correlated to the difference in the environments among four sites. The environments of sites A−D in 1,3-disilaallenes **1a** and **1b** are similar, but those in **1c** and **1d** are quite different from each other as shown in Figure 1. Thus, the differences among δ_A−δ_D in **1a** and **1b** are <10.1 and <15.3°, while those in **1c** and **1d** are >34.6 and >32.2°; in other words, for **1a** and **1b**, δ_X values are all around 90° but they are quite different from each other for **1c** and **1d**. The most and the least populated sites of M^2 in **1a** and **1b** are at A and C, which have the smallest and largest dihedral angles, respectively.

The larger environmental difference for **1c** and **1d** than that for **1a** and **1b** would be ascribed to the larger extent of the pyramidalization at the terminal Ge atoms than that at the terminal Si atoms, as discussed in the previous section.

NMR and UV−Vis Spectra. ^{1}H, ^{13}C, and ^{29}Si NMR spectra of trimetallaallenes **1a**−**1d** are very simple, indicating that eight trimethylsilyl groups, four ring methylenes, four ring quaternary

(18) Hurni, K. L.; Rupar, P. A.; Payne, N. C.; Baines, K. M. *Organometallics* **2007**, *26*, 5569.
(19) (a) Basch, H.; Hoz, T. In *The Chemistry of Organic Germanium, Tin and Lead Compounds*; Patai, S., Rappoport, Z., Eds; Chichester, U.K., 1995; p 1. (b) Desclaux, J. P. *At. Data Nucl. Data Tables* **1973**, *12*, 311.

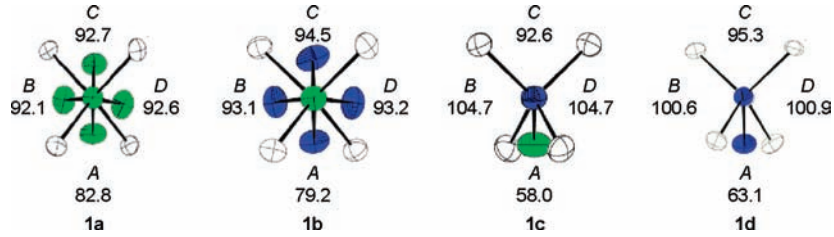

Figure 1. Skeletal structures ($C^1C^2M^1{=}M^2{=}M^3C^3C^4$) of **1a**−**1d** obtained by X-ray analysis at −100 °C shown as views projecting the molecules along the axis through the terminal M^1 and M^3 atoms (M^1, front side). Four quadrants divided by $C^1{-}M^1{-}C^2$ and $C^3{-}M^3{-}C^4$ planes are designated as sites A−D, which are characterized as dihedral angles $C^2{-}M^1{-}M^3{-}C^4$ (δ_A), $C^2{-}M^1{-}M^3{-}C^3$ (δ_B), $C^1{-}M^1{-}M^3{-}C^3$ (δ_C), and $C^1{-}M^1{-}M^3{-}C^4$ (δ_D); the dihedral angles are given in the structures. Si and Ge atoms are shown in green and blue colors, respectively.

Table 2. Site Occupancy Factors of M^2 Atom in **1a** and **1b** at Various Temperatures[a]

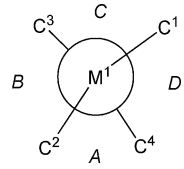

	1a				1b			
temp/°C	P_A	P_B	P_C	P_D	P_A	P_B	P_C	P_D
−180	−	−	−	−	0.950(1)	0.038(1)	0.000	0.012(1)
−150	0.755(2)	0.175(2)	0.000	0.070(2)	0.878(1)	0.076(1)	0.000	0.046(1)
−146	0.716(3)	0.185(3)	0.000	0.099(2)	−	−	−	−
−100	0.606(3)	0.208(3)	0.036(3)	0.150(3)	0.726(1)	0.136(2)	0.020(1)	0.117(1)
−50	0.523(6)	0.221(3)	0.066(3)	0.190(7)	0.616(7)	0.169(3)	0.048(2)	0.167(4)
0	0.460(3)	0.228(3)	0.095(3)	0.217(3)	0.533(2)	0.202(2)	0.078(1)	0.187(1)
ΔH^b	0	0.32	1.14	0.66	0	0.63	1.44	0.94
ΔS^c	0	−0.26	0.93	0.99	0	0.30	1.35	1.60

[a] $P_A{-}_D$ designate the site occupancy factors at sites A−D. [b] Enthalpy relative to that at site A, kcal mol^{-1}. [c] Entropy relative to that at site A, cal mol^{-1} K^{-1}.

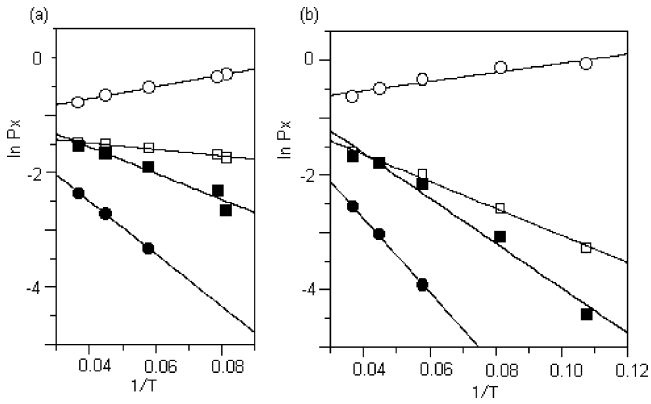

Figure 2. Plots of ln P_x vs $1/T$ for (a) **1a**, (b) **1b**; P_A (○), P_B (□), P_C (●), and P_D (■).

Table 3. NMR Chemical Shifts (δ) of Trimetallaallenes **1a**−**1d** in C_6D_6

	^1H		^{13}C			^{29}Si		
compound	CH_2[a]	$SiCH_3$[b]	CH_2	$C(q)$[c]	$SiCH_3$	$Si^{1,3}$	Si^2	$SiMe_3$
1a	2.00	0.39	34.3	27.2	3.3	196.9	157.0	1.6
1b	2.01	0.38	34.5	30.0	3.4	219.4	−	0.8
1c	2.12	0.36	39.1	35.9	3.9	−	236.6	1.2
1d	2.15	0.36	42.1	36.1	3.5	−	−	0.5

[a] Singlet (4H). [b] Singlet (36H). [c] Quaternary carbon.

Table 4. UV−Vis Spectral Data for **1a**−**1d**

compound	λ_{max}/nm (ε)			
1a	390 (21300)	430 (5000, sh)	480 (500, sh)	584 (700)
1b	409 (22000)	−	−	599 (1100)
1c	383 (28500)	432 (3800)	488 (2500)	612 (3100)
1d	380 (28100)	435 (3300)	496 (2800)	630 (5300)

carbons, and two terminal silicons in a molecule are all equivalent in solution. Chemical shifts and assignments of these signals are listed in Table 3.

Since the two π bonds of carbon allene (propadiene) are perpendicular to each other, the $\pi \rightarrow \pi^*$ absorption band maximum (λ_{max}) is found in the far-UV region similarly to that of ethylene.[20] The UV−vis absorption bands of **1a**−**1d** are found in the visible region and more complicated than those of the corresponding heavy ethylenes. (1) All these heavy allenes show at least two bands in the $\pi \rightarrow \pi^*$ band regions of disilenes and digermenes; the λ_{max}/nm(ε) values are listed in Table 4. The multiple $\pi \rightarrow \pi^*$ bands are observed as shoulders in **1a**, as a broad single band in **1b**, and as four distinct bands in **1c** and **1d**. (2) The most intense band in **1a**−**1d** is found at around 390 nm ($\varepsilon > 20\,000$), which is close to the $\pi \rightarrow \pi^*$ transition maxima for isolated tetraalkyldisilenes[21a,b] and digermenes.[21c] (3) The longest band maximum of **1a**−**1d** appears at around 600 nm with a small ε value. Both the λ_{max} and ε values of 1,3-digermaallenes **1c** and **1d** are significantly larger than those of 1,3-disilaallenes **1a** and **1b**. These spectral features in solution

(20) Sutcliffe, L. H.; Walsh, A. D. *J. Chem. Soc.* **1952**, 899.
(21) (a) Sekiguchi, A.; Maruki, I.; Ebata, K.; Kabuto, C.; Sakurai, H. *J. Chem. Soc., Chem. Commun.* **1991**, 341. (b) Masamune, S.; Eriyama, Y.; Kawase, T. *Angew. Chem., Int. Ed. Engl.* **1987**, *26*, 584. (c) Mochida, K.; Tokura, S. *Organometallics* **1992**, *11*, 2752.

Chart 2

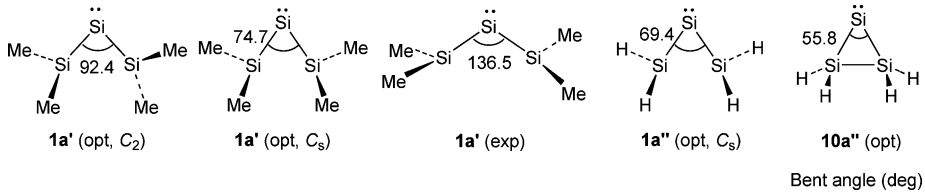

indicate that there is significant interaction between two double bonds of heavy allenes. The spectral feature is discussed further in the latter section on the basis of the TD-DFT calculations.

DFT Calculations for Model Heavy Allenes. A number of theoretical studies on the geometries and electronic structures of model trisilaallenes, tetramethyltrisilaallene ($Me_2Si{=}Si{=}SiMe_2$, **1a′**) and parent trisilaallene ($H_2Si{=}Si{=}SiH_2$, **1a″**), have been performed by us[7a] and the other authors.[22,23] We have shown in a communication[7a] that the optimized geometry of **1a′** having local C_2 symmetry [**1a′**(opt, C_2)] is remarkably bent with the $Si^1{-}Si^2{-}Si^3$ bent angle of 92.4° and two C_2Si planes are slightly twisted from each other with the dihedtral angle of 26.6° at the B3LYP/6-31+G(d,p) level (Chart 2). Apeloig et al.[22a,b] and Veszprémi et al.[22c] have investigated independently the structure and bonding of $H_2Si{=}Si{=}SiH_2$ (**1a″**) and related compounds theoretically. The Si−Si−Si bent angle of **1a″** at the optimized geometry [**1a″**(opt)] with C_s symmetry is only 67.1−70.4° depending on the computational level. Trisilacyclopropylidene structure **10a″** is 2.7 kcal mol^{-1} higher in energy than **1a″**(opt, C_s) (Chart 2).[22c]

The two research groups have investigated also **1a′** and found that the bent angle is 74.2° at the optimized structure having C_s symmetry [**1a′**(opt, C_s)] at the B3LYP/6-31G(d,p) level. Similarly, our latest calculations for **1a′**(opt, C_s) at the B3LYP/6-31+G(d,p) level gave the bent angle of 74.7° with slightly higher energy (0.3 kcal mol^{-1}) than **1a′**(opt, C_2).[16] The two optimized structures with C_s and C_2 symmetry are derived by disrotatory and conrotatory rotation of the two terminal Me_2Si substituents from bent $Me_2Si{=}Si{=}SiMe_2$ having four coplanar methyl carbons to the Si_3 plane, respectively. Further disrotatory rotation from **1a′**(opt, C_s) leads to tetramethyltrisilacyclopropylidene [**10a′**(opt)], which is 3.7 kcal mol^{-1} higher in energy than **1a′**(opt, C_s).[16]

Inspection of the Kohn−Sham orbitals of **1a′**(opt, C_2) and **1a′**(opt, C_s) indicates that these are described formally as zwitterionic structures with π cation−n anion pair.[24] As shown in the Supporting Information,[16] the HOMO, LUMO, and LUMO+1 of **1a′**(opt, C_2) are symmetric, antisymmetric, and symmetric π-type orbitals with respect to the pseudo-symmetry plane through the Si^2 atom and perpendicular to the Si_3 plane, and hence, the MO feature of the cationic part is similar to that of allylic cation. On the other hand, the HOMO and LUMO of **1a′**(opt, C_s) are both symmetric with respect to the symmetry plane, indicating significant π bonding between Si^1 and Si^3 atoms. Because the π cation part of **1a′**(opt, C_2) and **1a′**(opt, C_s) is similar to allylium and cyclopropenylium cation, respectively, they are characterized as zwitterionic (allylium) (ZA) and zwitterionic (cyclopropenylium) (ZC) structures. The close relative stability between **1a′**(opt, C_s) and **1a′**(opt, C_2) would be explained by considering that the ZC structure is stabilized more than the ZA structure by the bonding 1,3-Si interaction but destabilized by the enhanced steric repulsion between the substituents and the bond angle strain. Actually, the corresponding heavy cyclopropylidene **10a′** is less stable than **1a′**(opt, C_s), even though the former has a σ bond between the 1,3-Si atoms.

The experimentally observed skeletal geometry of **1a** is quite different from those of the zwitterionic structures (ZA and ZC) and the bent planar allenic structure of small cyclic carbon allenes.[24] The Si−Si−Si bond angle (136.5°) is much larger than those found for optimized **1a′**, and the two C_2Si planes in **1a** are almost perpendicular to each other as found in carbon allenes. As shown in Figure 3, the Kohn−Sham frontier orbitals for **1a′**(exp) indicate that in-plane and out-of-plane p-type orbitals on the central Si atom interact effectively with two pπ-type orbitals on terminal two Si atoms that are nearly perpendicular to each other, and hence, the electronic structure is different from those of ZA and ZC.[16] The structure of **1a** and **1a′**(exp) should be assigned as a bent perpendicular allene; the two planes which bisect $C^1{-}M^1{-}C^2$ and $C^3{-}M^3{-}C^4$ planes in the allene are maintained to be perpendicular to each other as found in a linear allene,[24] while the two trans-bent Si=Si bonds

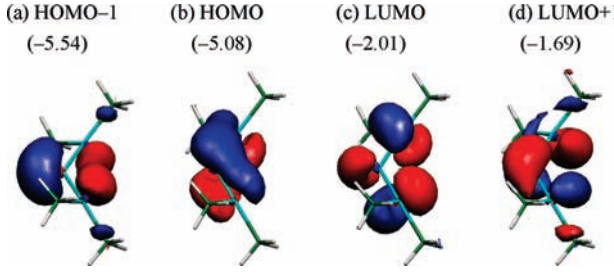

Figure 3. Frontier Kohn−Sham orbitals and their energy levels in electronvolts of tetramethyltrisilaallene **1a′**(exp) calculated at the B3LYP/6-311++G(d,p) level.

(22) (a) Kosa, M.; Karni, M.; Apeloig, Y. *J. Am. Chem. Soc.* **2004**, *126*, 10544. (b) Kosa, M.; Karni, M.; Apeloig, Y. *J. Chem. Theory Comput.* **2006**, *2*, 956. (c) Veszprémi, T.; Petrov, K.; Nguyen, C. T. *Organometallics* **2006**, *25*, 1480.

(23) Very recently, DFT calculations for trigermaallenes and related germaallenes have been reported: Sk, M. A.; Xi, H.-W.; Lim, K. H. *Organometallics* **2009**, *28*, 3678.

(24) Terms of "bent allenic", "biradical", and "zwitterionic" have been used for strained cyclic allenes by Johnson et al.,[25] where ring constraints bend the allenes and exert torsion toward a planar arrangement of the substituents. The twist angle defined as a $H{-}C^1{-}C^2{-}C^3$ dihedral angle for 1,2-cyclohexadiene is calculated to be 142.2°,[25c] suggesting the allene is possibly assigned as bent allenic. The four- and five-membered cyclic 1,2-dienes synthesized by Bertrand et al.[11] are bent planar allenes, and hence, the allenes are zwitterionic or biradical type, because the in-plane (n-type) and out-of-plane (π-type) orbitals should be orthogonal to each other. On the other hand, heavy allenes **1a**−**1d** are free from ring strain. The $C^1{-}Si^1{-}C^2$ and $C^3{-}Si^3{-}C^4$ planes of **1a** and **1b** are almost perpendicular to each other and share the Si^1---Si^3 axis, similarly to carbon allene. This type of bent allenes is defined here as bent perpendicular allene, which may not be a molecular local minimum but found as a stationery point of the dynamic structure in the solid state. The geometry of **1c** and **1d** is more complicated due to the pyramidalization at the terminal germanium atoms but has essentially similar characteristics to those of **1a** and **1b**.

(25) (a) Johnson, R. P. *Chem. Rev.* **1989**, *89*, 1111. (b) Schmidt, M. W.; Angus, R. O.; Johnson, R. P. *J. Am. Chem. Soc.* **1982**, *104*, 6838. (c) Daoust, K. J.; Hernandez, S. M.; Konrad, K. M.; Mackie, I. D.; Winstanley, J., Jr.; Johnson, R. P. *J. Org. Chem.* **2006**, *71*, 5708.

Chart 3

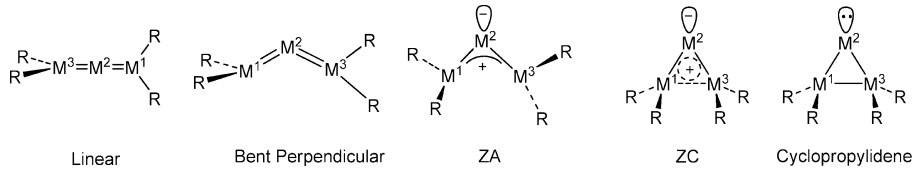

share the central Si atom and the significant electronic interaction exists between the two π-type bonds. How the bent perpendicular structure of **1a** is built up will be discussed using the PMO theory in a latter section. The wide Si−Si−Si bond angle of **1a** is reported to be mostly reproduced when the real system of **1a** is optimized; the angle is 130.2° at the B3LYP/6-31G(d) level[22c] and 135.7° at the BP86/TZVPP level.[26] The results suggest that the potential surface of the skeletal Si−Si−Si bending of trisilaallene is rather shallow, and hence, the bond angle is sensitive to the steric repulsion between terminal substituents.[27] It should be also noted that the geometric and electronic structure of trisilaallene is modified from zwitterionic to bent perpendicular allenic with widening the bond angle.[28]

The theoretical calculations have revealed that at least five structures, linear, bent perpendicular, ZA, ZC, and cyclopropylidene, should be considered as isomers of carbon and heavy allenes, as shown in Chart 3, and the relative energies remarkably depend on skeletal elements and substituents. For **1a′**−**1d′**, ZA, ZC, and cyclopropylidene structures are the local minima but linear and bent perpendicular allenic structures are not located as minima. The structure of bent perpendicular allene is taken as that having skeletal characteristics of **1a**−**1d**.

To elucidate the structure of **1a**−**1d** in solution, the GIAO calculations for ^{29}Si NMR chemical shifts were performed for various geometries of $Me_2M{=}M'{=}MMe_2$ [**1a′** (M = M′ = Si), **1b′** (M = Si, M′ = Ge), and **1c′** (M = Ge, M′ = Si)] at the GIAO/B3LYP/6-311+G(2df,p)//B3LYP/6-31+G(d,p) level. In Table 5, the calculated ^{29}Si NMR chemical shifts for various structures of **1a′**−**1c′** are summarized. Although the structure of **1a′**−**1c′** in solution may not be the same as that in the solid state, it should be noted that the experimental ^{1}H, ^{13}C, and ^{29}Si NMR spectral patterns of **1a**−**1d** are very simple and highly symmetric and, hence, only in accord with those for linear allenes or the dynamic equilibriums among bent perpendicular allenic isomers A−D in Figure 1. Because the geometries of isomers A−D in a bent perpendicular allene are expected to be close to each other, the chemical shifts calculated for isomer A would be taken roughly as the average of the shifts among A−D. The calculated ^{29}Si chemical shifts for linear as well as ZA and ZC allenes are not compatible with those observed experimentally. On the other hand, the chemical shifts at Si^2 and Si^{1,3} of **1a** and at Si^{1,3} of **1b** are in accord with those calculated for bent perpendicular allenic structures of **1a′** and **1b′**. Whereas the Si^2 shift for **1c** is not sufficiently in accord with that calculated for the bent perpendicular structure of **1c′**, the reason would be ascribed in part to the significant structural difference among isomers A−D. As a whole, the structure of **1a**−**1d** in solution is taken to be bent perpendicular allenic with rapid interconversion among isomers A−D, similar to that in the solid state.

Table 5. Theoretical ^{29}Si Chemical Shifts of Heavy Tetramethylallenes[a] at Various Structures[b]

	1a′		**1b′**	**1c′**
structure[c]	Si^2	Si^{1,3}	Si^{1,3}	Si^2
experimental	157.0[d]	196.9[d]	219.4[e]	236.6[f]
bent perpendicular[g]	161.2	202.0, 209.0	231.2, 230.8	271.8
linear[h]	210.0	98.3	98.5	245.0
ZA	38.7	354.8	378.3	40.4
ZC	198.1	199.1	184.3	241.1

[a] **1a′**, $Me_2Si{=}Si{=}SiMe_2$; **1b′**, $Me_2Si{=}Ge{=}SiMe_2$; **1c′**, $Me_2Ge{=}Si{=}GeMe_2$. [b] Calculated at the GIAO/B3LYP/6-311+G(2df,p)//B3LYP/6-31+G(d,p) level, ppm. [c] For definition of the structures, see Chart 3. [d] ^{29}Si chemical shift for **1a** in benzene-d_6. [e] ^{29}Si chemical shift for **1b** in benzene-d_6. [f] ^{29}Si chemical shift for **1c** in benzene-d_6. [g] Geometry of $C_2M{=}M'{=}MC_2$ moiety of **1a′**, **1b′**, and **1c′** is fixed to that determined by X-ray crystallography for isomer A of **1a**, **1b**, and **1c**, respectively. The chemical shifts for isomers A−D are assumed to be close to each other because of the similarity of their structures. The X-ray structure is unsymmetric with two different M=M bond distances, and hence, the Si^1 and Si^3 chemical shifts are calculated to be slightly different. [h] Geometry with two imaginary frequencies is optimized under the constraint of linear arrangement of M−M′−M skeleton.

UV−vis transition energies and their oscillator strengths of **1a′**−**1d′** calculated at the TD-B3LYP/6-311++G(d,p) level are also found to be remarkably dependent on the structure of heavy allenes.[16] The theoretical calculations for **1a′**(exp) indicate that there are four bands in the $\pi \rightarrow \pi^*$ band region assignable to HOMO(π) → LUMO(π^*) (band i, weak), HOMO(π)−1 → LUMO(π^*) (band ii, weak), HOMO(π) → LUMO(π^*)+1 (band iii, strong), and HOMO(π)−1 → LUMO(π^*)+1 (band iv, medium) transitions, being consistent with the existence of two π HOMOs and two π^* LUMOs in the bent perpendicular allene (Figure 3); the transition energies are in the order band i < band ii < band iii < band iv. The experimental spectral feature for heavy allenes **1a**−**1d** (Table 4) is qualitatively in accord with those calculated for bent perpendicular structures of **1a′**−**1d′**. It is noteworthy that the remarkable increase of intensity of the longest wavelength band in the order **1a** < **1b** < **1c** < **1d** is reproduced by the present calculations for the bent perpendicular structures of **1a′**−**1d′**. The origin of the release of the forbidden nature in germanium congeners of heavy allenes would be an interesting issue to be unveiled.

Qualitative MO Description of Bonding in Heavy Allenes. The goal of this study is to analyze using qualitative MO theory the origin of the remarkable difference in bonding and structure between carbon and heavy allenes as shown by the experimental and computational results. The difference should be the reflection of the different properties of s and p orbitals between carbon and heavy group-14 elements, because valence electronic configuration of all group-14 elements is the same ns^2np^2, where n is principal quantum number. Several remarkable and important differences in properties between carbon and heavier group-14 elements have been discussed in the literature as

(26) (a) Takagi, N.; Shimizu, T.; Frenking, G. *Chem.—Eur. J.* **2009**, *15*, 3448. (b) Takagi, N.; Shimizu, T.; Frenking, G. *Chem.—Eur. J.* **2009**, *15*, 8593.

(27) In conformity with this explanation, the distance between M1 and M3 atoms is similar among **1a**−**1d**: 4.054, 4.093, 4.039, and 4.080 Å for **1a**, **1b**, **1c**, and **1d**, respectively.

(28) See ref 22c for another view for the bond angle dependence of the electronic structure of trisilaallene.

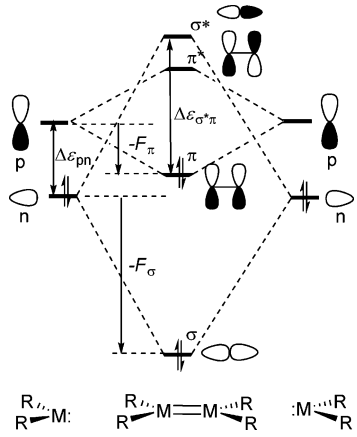

Figure 4. Schematic representation of orbital interactions between two divalent species of group-14 elements (M = Si, Ge, Sn).

follows:[2b,19,29] The energies of 2s and 2p orbitals (−19.39 and −11.07 eV) are much lower than those of *n*s and *n*p orbitals with $n > 2$ (−14.84 and −7.57 eV for Si and −15.52 and −7.29 eV for Ge), while the energy difference between 2s and 2p orbitals is even larger than those between *n*s and *n*p orbitals ($n > 2$); the *n*s/*n*p separation is 8.32, 7.27, and 8.23 eV for C, Si, and Ge. Whereas the orbital size of both *n*s and *n*p defined as the orbital radii of maximal electron density (r_{ns} and r_{np}) increases with increasing *n*, the difference Δr_n ($=r_{np} - r_{ns}$) for carbon ($n = 2$) is exceptionally small compared to those for Si and Ge; $\Delta r_2 = -0.2$ pm but $\Delta r_n > 20$ pm for $n > 2$.[2b,30a] The smaller value of Δr_2 than those of Δr_n ($n > 2$) is considered to be responsible for the effective sp hybridization in carbon and hybridization defects[29,30] in the heavier elements.

According to the CGMT model,[5,6] the geometry of heavy alkenes ($R_2M{=}MR_2$) is correlated with the relationship between the singlet−triplet energy difference ($\Delta E_{ST} = E_T - E_S$) of the corresponding metallylene R_2M: and the sum of σ and π bond energies ($E_{\sigma+\pi} = E_\sigma + E_\pi$). Thus, a heavy alkene is planar if $(-1/2)E_{\sigma+\pi} < \Delta E_{ST} < (1/4)E_{\sigma+\pi}$, while it is trans-bent if $(1/4)E_{\sigma+\pi} < \Delta E_{ST} < (1/2)E_{\sigma+\pi}$; if $\Delta E_{ST} > (1/2)E_{\sigma+\pi}$, the M=M double bond is not formed anymore. The criterion is useful but seems to need annotations. Although the MOs of a heavy ethylene ($H_2M{=}MH_2$) are composed of those of the corresponding two metallylenes (H_2M:) in the MO arguments of the CGMT model, the *n*p orbital energy difference in H_2M: ($\Delta\varepsilon_{pn}$; $\varepsilon_p - \varepsilon_n > 0$) and the orbital interaction energies between two *n* and between two p orbitals (F_σ and F_π, respectively, <0) are replaced to the singlet−triplet energy difference $-\Delta E_{ST}$ and a half of the bond energies $-E_\sigma$ and $-E_\pi$ to maintain the compatibility with the explanation using the valence bond (VB) theory (Figure 4).[5c] Since in the framework of the PMO theory,[8] MOs of a system are built up through the interaction between MOs of the fragments, this displacement is rather confusing. In this sense, the condition that a heavy ethylene is planar should be expressed alternatively as $F_{\sigma+\pi} < \Delta\varepsilon_{pn} < -(1/2)F_{\sigma+\pi}$; $F_{\sigma+\pi} = F_\sigma + F_\pi$. We realize however that $\Delta\varepsilon_{pn}$ in *singlet* H_2M: is rather large irrespective of M and even larger for M = C than that for M = Si and Ge; $\Delta\varepsilon_{pn}$ is calculated to be 11.5, 9.14, and 9.05 eV for optimized singlet:CH_2, :SiH_2, and :GeH_2, respectively,

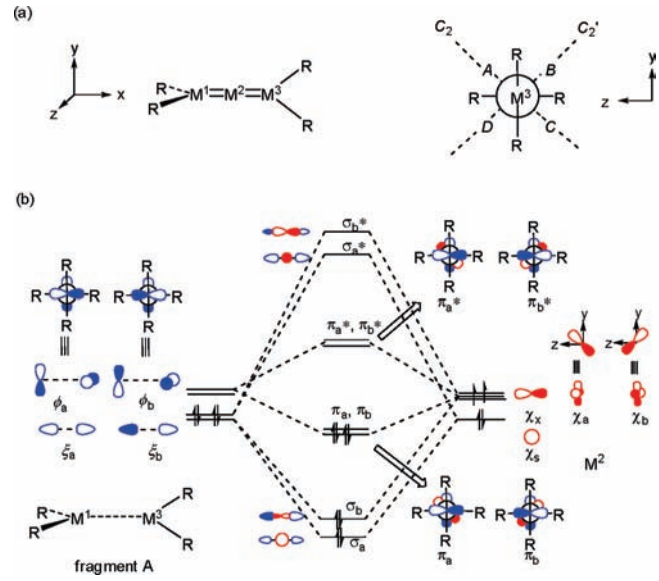

Figure 5. (a) Structure of a linear perpendicular allene $R_2M^1{=}M^2{=}M^3R_2$ (D_{2d}). A Newmann-like projection of the D_{2d} allene as viewed along the axis through M^1 (back) and M^3 (front) atoms, where M^2 atom is on the same axis, is shown in the right, together with two C_2 axes (C_2 and C_2' axes) of the D_{2d} molecule. Four quadrants separated by $R{-}M^1{-}R$ and $R{-}M^3{-}R$ planes are labeled as A−D in the figure. (b) General description of the MOs of a D_{2d} allene constructed by the orbital interaction between a R_2M^1---M^3R_2 fragment and a central M^2 atom. Orbitals on M^1 and M^3 and those on M^2 are shown in blue and red, respectively. For simplicity, only orbitals constructing the $M^1{=}M^2{=}M^3$ skeleton, i.e., lone-pair *n* and vacant p orbitals on M^1 and M^3 atoms, are taken into account, in addition to atomic orbitals on M^2 atom. The ξ_a and ξ_b orbitals are positive and negative combinations of two *n* orbitals on M^1 and M^3, respectively. Similarly, the ϕ_a and ϕ_b orbitals are positive and negative combinations of two p orbitals on M^1 and M^3. Three degenerate atomic p orbitals, χ_x, χ_y, and χ_z on M^2, are replaced by an equivalent set of orbitals, χ_x, χ_a [$=1/\sqrt{2}(\chi_y + \chi_z)$], and χ_b [$=1/\sqrt{2}(\chi_y - \chi_z)$], the latter two of which are taken to be symmetric and antisymmetric combination about the C_2 axis shown in (a) (right).

at the HF/6-311+G(d,p)//B3LYP/6-311+G(d,p) level.[16,31] This means that the planarity of (heavy) ethylenes is not simply correlated with the $\Delta\varepsilon_{pn}$. On the other hand, because *n*s and *n*p orbitals defuse with increasing *n*, the interaction energies $-F_\sigma$ and $-F_\pi$ and, hence, $-F_{\sigma+\pi}$ of heavy ethylenes will be smaller than those of ethylene.[5] Furthermore, because $-F_\sigma$ of heavy ethylenes includes the contribution of *n*s orbitals, F_σ/F_π of heavy ethylenes will be reduced relative to that of ethylene due the hybridization defects. Because of the larger $F_{\sigma+\pi}$, the planarity of substituted ethylenes is much less sensitive to $\Delta\varepsilon_{pn}$ than that of heavy ethylenes. The above discussion is good in accord with the fact that though the ΔE_{ST} of F_2C: (57.6 kcal mol^{-1})[32] is even larger than that of GeH_2 (23.1 kcal mol^{-1}),[33] $F_2C{=}CF_2$ is a planar molecule, while $H_2Ge{=}GeH_2$ is trans-bent.

Molecular orbitals (MO) of a linear perpendicular $R_2M^1{=}M^2{=}M^3R_2$ (M^1, M^2, and M^3 are the same group-14 elements) with D_{2d} symmetry can be derived by the interaction between the orbitals of a fragment involving remote two R_2M groups (fragment A) and those of the central M^2 atom as schematically shown in Figure 5. For simplicity, only lone-pair *n* and vacant

(29) (a) Kutzelnigg, W. *Angew. Chem., Int. Ed. Engl.* **1984**, *23*, 272. (b) Kutzelnigg, W. *J.Mol. Struct.: THEOCHEM* **1988**, *169*, 403.
(30) (a) Nagase, S. In *The Transition State*; Fueno, T., Ed.; Kodansha: Tokyo, 1999; p 147. (b) Kaupp, M.; Schleyer, P. v. R. *J. Am. Chem. Soc.* **1993**, *115*, 1061.
(31) Because there is geometry change between singlet and triplet methylenes, ΔE_{ST} may not be parallel to $\Delta\varepsilon_{pn}$. In methylene and heavy methylenes optimized at the singlet state, the H−M−H bond angle is close to that found in the corresponding ethylenes. Though the $\Delta\varepsilon_{pn}$ values may be unreliable and dependent on the theoretical levels, the tendency among methylene and heavy methylenes is maintained.

p orbitals on M^1 and M^3 atoms are taken into account for fragment A. The two degenerate *n* orbitals of fragment A may be replaced by ξ_a and ξ_b orbitals which are symmetric and antisymmetric orbitals with respect to a designated C_2 axis through M^2 atom (Figure 5). Similarly, the two degenerate symmetry-adapted p orbitals of fragment A are described as ϕ_a and ϕ_b orbitals as shown in Figure 5. Three degenerate atomic p orbitals, χ_x, χ_y, and χ_z, on M^2 are replaced by an equivalent set of orbitals, χ_x, χ_a [$=1/\sqrt{2}(\chi_y + \chi_z)$], and χ_b [$=1/\sqrt{2}(\chi_y - \chi_z)$], the latter two of which are taken to be symmetric and antisymmetric with respect to the C_2 axis. The symmetry-allowed interaction between orbitals on fragment A and atomic orbitals on M^2 will form the bonding σ (σ_a and σ_b), antibonding σ^* (σ_a^* and σ_b^*), bonding π (π_a and π_b), and antibonding π^* (π_a^* and π_b^*) orbitals as shown in Figure 5. The qualitative MO diagram obtained here is in good agreement with the known MO description of parent allene.[34] Because the σ^* (σ_a^* and σ_b^*) and π (π_a and π_b) orbitals of carbon allene are well separated, the $\pi-\sigma^*$ mixing caused possibly by the bending of the C−C−C skeleton would be too small to stabilize the system. Instead, the bending may lead to the destabilization of the system due to the reduced overlap between ϕ_a (ϕ_b) and χ_a (χ_b) and between ξ_a (ξ_b) and χ_s (χ_x).

On the other hand, if M is a heavy group-14 element like Si, the overlap between ξ_a and χ_s would be relatively poor due to the intrinsically smaller size of χ_s than χ_x, χ_y, and χ_z. Hence, the energy separation between σ_a and σ_a^*, and in turn, the energy separation between σ_a^* and π_a (and π_b) in heavy allenes, would be much smaller than those in carbon allene. The small energy separation would cause the second-order Jahn−Teller distortion from D_{2d} to C_2 associated with the effective mixing between σ_a^* and one of π_a and π_b orbitals ($\pi-\sigma^*$ distortion) to stabilize the system as shown in Figure 6a. Because there are two C_2 axes through M^2 in a D_{2d} allene, the deformation to a bent perpendicular allene (C_2 allene) may occur in the four directions along the two C_2 axes; that is, four isomers A−D, where M^2 is located in quadrants A−D, respectively, may form as experimentally observed. The degenerate π_a and π_b orbitals in D_{2d} allene will be modified by the deformation to give degenerate π_a' and π_b' orbitals in C_2 allene whose energies are a little higher than those of π_a and π_b because of the reduced overlap between ϕ_a and χ_a (Figure 5b). However, for example, in isomer A, both π_a' and $\sigma_a'^*$ (modified σ_a^* orbital in C_2 allene) are symmetric with respect to rotation around the C_2 axis and, hence, can mix with each other, while no mixing is expected between $\sigma_a'^*$ and π_b' because π_b' is antisymmetric about the C_2 rotation; the π_a' and σ_a^* orbitals are modified by the mixing to be ($\pi_a' + c\sigma_a^*$) and ($\sigma_a^* - c'\pi_a'$), respectively, where c and c' are the mixing coefficients. The orbital mixing mode in isomer A is shown schematically in Figure 6b. The χ_s and ξ_a components of σ_a^* (Figure 5b) mix both in-phase into ϕ_a and χ_a components of π_a', respectively, to stabilize π_a'. The s/p orbital mixing[8] at M^2 is thus

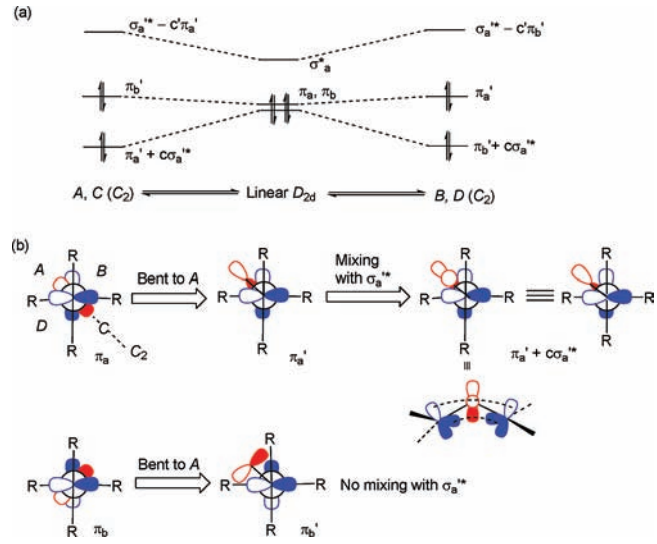

Figure 6. (a) Schematic $\pi-\sigma^*$ orbital mixing diagram for the deformation of linear D_{2d} allene to bent C_2 allene isomers A−D. The energy levels of π_a' and π_b' in a C_2 allene would be a little higher than those of π_a and π_b because the χ_a/ϕ_a and χ_b/ϕ_b overlaps in the C_2 allene are less effective than those in D_{2d} allene. In isomers A and C, π_a' and π_b' are symmetric and antisymmetric, respectively, about the C_2 rotation; σ_a^* that is symmetric to the rotation mixes only into π_a' to stabilize the orbital. Similarly, the $\pi-\sigma^*$ mixing in isomers B and D leads to the stabilization of π_b'. The mixing coefficients c and c' are small positive numbers. (b) Above $\pi-\sigma^*$ orbital mixing in isomer A shown schematically. Orbitals on M^1 and M^3 and those on M^2 are shown in blue and red, respectively.

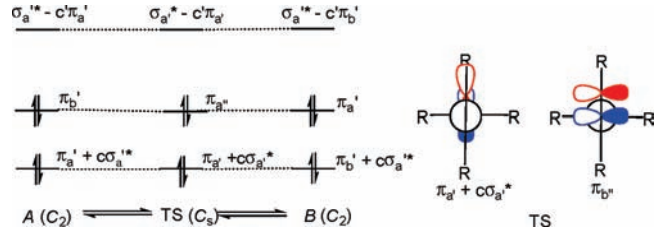

Figure 7. Schematic MO correlation diagram for the rotation of M^2 atom around the M^1---M^3 axis (path I). The isomerization between isomers A and B is shown as representative. Similar diagrams are obtained for the isomerization between B and C, between C and D, and between D and A. Orbitals on M^1 and M^3 and those on M^2 are shown in blue and red, respectively.

introduced in the perturbed π_a' orbital. The shape of $\pi_a' + c\sigma_a'^*$ and π_b obtained qualitatively by the $\pi-\sigma^*$ mixing is in good accord with the Kohn−Sham HOMO and HOMO−1 calculated for **1a′**(exp)[7a] as shown in Figure 3, and hence, the structure of **1a′** (exp) is characterized as bent perpendicular allene.

The temperature-dependent dynamic disorder at a low-temperature region found experimentally in the crystals of **1a** and **1c** suggests that the energy barriers separating between isomers A−D are very low. There are two possible mechanisms for the isomerization anticipated, the rotation of M^2 around the M^1---M^3 axis (A → B → C → D → A and its inverse, path I) and isomerization via the deformation of a bent C_2 allene to linear D_{2d} allene to another bent C_2 allene (path II). As shown typically for the isomerization between A and B in Figure 7, at the transition state (TS) via rotation (path I), M^2 atom is in the R−M^3−R plane and the molecular symmetry changes to C_s. At the TS, there are two bonding π orbitals, $\pi_{a'}$ and $\pi_{a''}$ which are symmetric and antisymmetric with respect to the molecular symmetry plane (σ_h). By mixing with $\sigma_{a'}^*$, $\pi_{a'}$ is stabilized, while $\pi_{a''}$ is intact. Because the extent of the $\pi-\sigma^*$ mixing in TS will be similar to that in A and B, the barrier between

(32) At the MP4/6-311G(2df)//MP2/6-31G(d) level. Gobbi, A.; Frenking, G. *J. Chem. Soc., Chem. Commun.* **1993**, 1162.
(33) At the CASSCF level using relativistic CI ECP (RCI) with inclusion of spin−orbit coupling effects. Balasubramanian, K. *J. Chem. Phys.* **1988**, *89*, 5731.
(34) Jorgensen, W. L.; Salem, L. *The Organic Chemist Book of Orbitals*; Academic Press: New York, 1973.
(35) (a) Tonner, R.; Oexler, F.; Neumueller, B.; Petz, W.; Frenking, G. *Angew. Chem., Int. Ed.* **2006**, *45*, 8038. (b) Tonner, R.; Frenking, G. *Angew. Chem., Int. Ed.* **2007**, *46*, 8695.
(36) (a) Kira, M.; Yauchibara, R.; Hirano, R.; Kabuto, C.; Sakurai, H. *J. Am. Chem. Soc.* **1991**, *113*, 7785. (b) Kira, M.; Ishida, S.; Iwamoto, T.; Yauchibara, R.; Sakurai, H. *J. Organomet. Chem.* **2001**, *636*, 144.

Chart 4

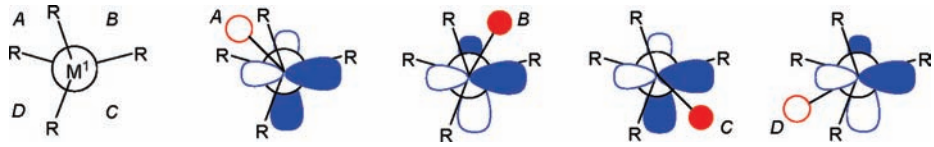

A and B would be low and determined mostly by enhanced steric repulsion between M^2 and R on M^3. The full rotation via path I will occur easily because the other three TSs during the rotation are identical to the TS between A and B. On the other hand, the isomerization via path II should have a higher barrier because no $\pi-\sigma^*$ mixing is expected at the D_{2d} allene as analyzed above (Figure 5). The present analysis suggests that the isomerization among A−D occurs through the rotation of M^2 around the M^1---M^3 axis rather than through the deformation of C_2 allenes to linear D_{2d} structure.

Next, our discussion is extended to heavy allenes with significant pyramidalization at the terminal atoms M^1 and M^3. The pyramidalization causes the mixing of the *n*p and *n*s orbitals at M^1 and M^3 and modifies the fragment π-type orbitals in Figure 5 (ϕ_a and ϕ_b) to the combination of the corresponding sp^x-hybrid orbitals (ϕ_a' and ϕ_b'). In this situation, the environment among quadrants A−D is expected to be considerably different from each other. As shown in Chart 4, when M^2 atom is at quadrants A and C, the $\pi-\sigma^*$ mixing involves the overlap of χ_s component of σ_a^* with the two front lobes and the two back lobes of ϕ_a' component of π_a, respectively, while when M^2 is at quadrants B and D, the $\pi-\sigma^*$ mixing involves the overlap of χ_s with the front and back lobes of ϕ_b'. On the other hand, the interaction between ξ_a and χ_a will be independent of the rotation of M^2 around the M^1---M^3 axis.

Because the front lobes are larger than the back lobes but face outwardly from the M−M−M framework, the $\pi-\sigma^*$ mixing is expected to be effective in the order A > B ∼ D > C. This order is in accord with the order of the occupancy factor in **1a** and **1b** and explains why M^2 is found only at quadrant A in **1c** and **1d**.

To analyze the reason why trisilaallenes with smaller substituents are zwitterionic, the discussion based on the PMO theory is extended to the $\pi-\sigma^*$ distortion of a planar linear allene (D_{2h}). An MO diagram for a $R_2M{=}M{=}MR_2$ (D_{2h}) molecule is again composed of a fragment with remote two coplanar R_2M groups and a central M^2 atom as schematically shown in Figure 8. At the D_{2h} allene, the π_{a2} (=ϕ_{a2}) and π_{a1} (=χ_z) orbitals constitute degenerate nonbonding orbitals, and hence, the D_{2h} carbon allene will be triplet and much less stable than the linear perpendicular allene (D_{2d} allene). However, in a heavier planar linear allene, the σ_{a1}^* orbital is low-lying due to the hybridization defects. Stabilization of the system due to the mixing of σ_{a1}^* orbital into π_{a1} orbital is attained by the deformation of D_{2h} allene to C_{2v} allene, i. e., movement of M^2 atom along the C_2 axis shown in Figure 8.

The $\pi-\sigma^*$ mixing in a bent planar C_{2v} allene is shown schematically in Figure 9. The $\pi-\sigma^*$ mixing would be more effective than that in a bent perpendicular C_2 allene (Figures 5 and 6), because π_{a1} is nonbonding and higher-lying than bonding π_a (π_b) orbitals of D_{2d} allene and because π_{a1} is localized at M^2 atom. In the C_{2v} allene, the $\pi_{a1} + \sigma_{a1}^*$ orbital formed by the mixing is stabilized to be fully occupied and π_{a2} becomes vacant; the electronic configuration is regarded as zwitterionic. The $\pi-\sigma^*$ mixing is similar to that in heavy carbenes,[10] and the geometry may be strongly bent as far as the bending is hampered by the steric repulsion between the substituents. As seen in the Kohn−Sham orbitals of $Me_2Si{=}Si{=}SiMe_2$ with C_2 and C_s symmetry,[16] the $\pi_{a1} + \sigma_{a1}^*$ orbital is lower than π_{b2}; in the C_s

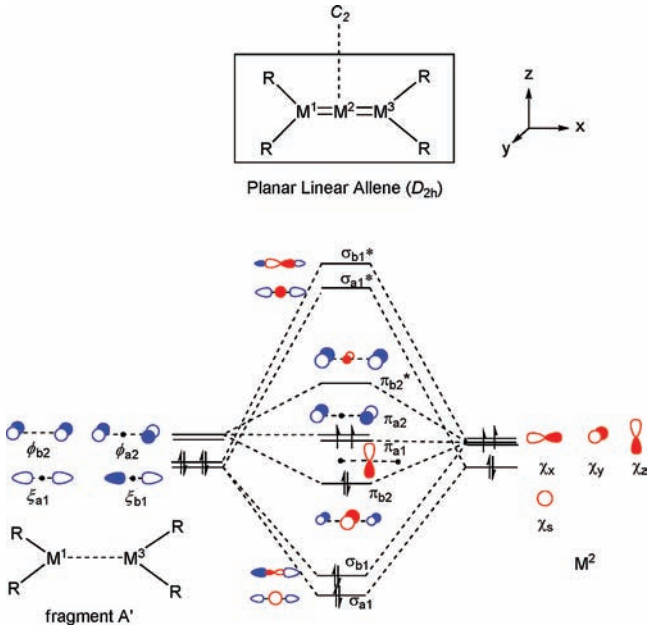

Figure 8. Description of the MOs of a planar linear allene $R_2M^1{=}M^2{=}M^3R_2$ constructed from the orbital interaction between fragment A′ and M^2 atom. For simplicity, only orbitals constructing the $M^1{=}M^2{=}M^3$ skeleton are taken into account. Orbitals on M^1 and M^3 and those on M^2 are shown in blue and red, respectively.

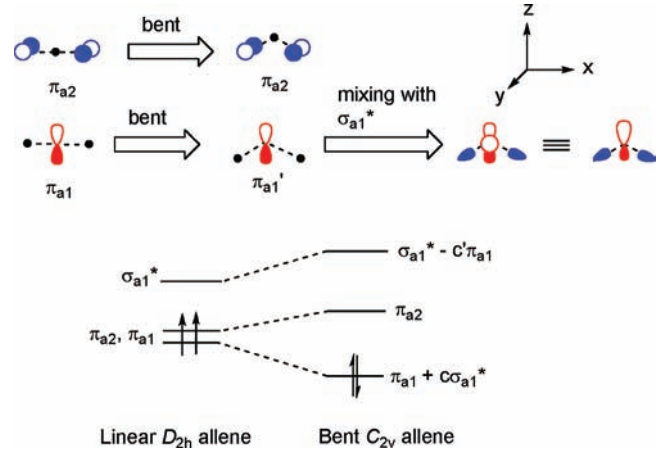

Figure 9. Schematic representation of $\pi-\sigma^*$ orbital mixing associated with the deformation from D_{2h} allene to C_{2v} allene. Orbitals on M^1 and M^3 and those on M^2 are shown in blue and red, respectively.

Chart 5

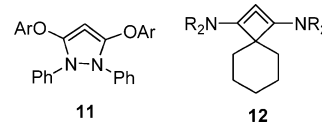

11 **12**

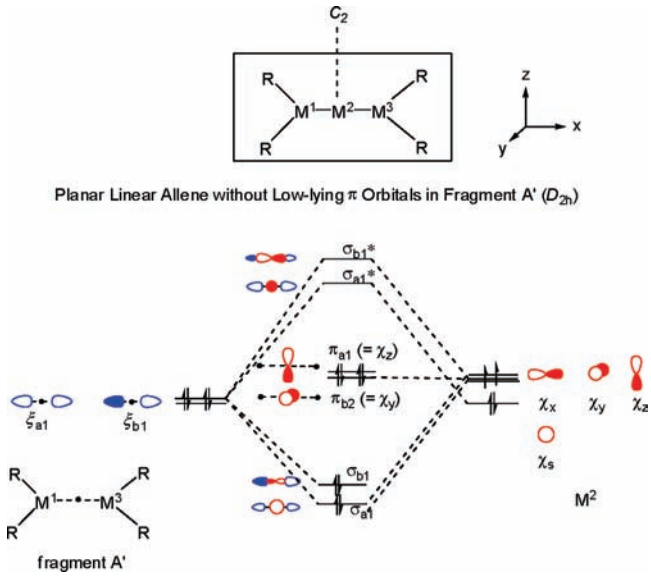

Figure 10. Orbital interaction diagram of a heavy allene without low-lying vacant orbitals at the R_2M. Orbitals on M^1 and M^3 and those on M^2 are shown in blue and red, respectively. In this figure, only the planar heavy allene is considered, but a similar diagram is obtained for the perpendicular one shown in Figure 5. The molecule has two degenerate nonbonding orbitals (χ_y and χ_z) at the linear geometry, but χ_y is stabilized by $\pi-\sigma^*$distortion to a bent structure. The barrier of rotation around M^1-M^2 and M^2-M^3 is suggested to be low in this molecule.

trisilaallene with a narrower bent angle, the mixed orbital is even lower than the σ_{b1} orbital, and in addition, the π_{b2}* orbital becomes the LUMO due to the stabilization of π_{b2} and destabilization of π_{a2} by the through-space 1,3-interaction.

Preference between the bent perpendicular C_2 geometry found experimentally and the bent planar C_{2v}-like geometry as found theoretically will be determined by the steric hindrance between substituents. A less sterically hindered heavy allene can be bent strongly at the approximately planar geometry, while twisting to the perpendicular geometry is required for significant bending of a heavy allene with bulky substituents.

It will be interesting to discuss the unusual electronic structure of bent allenes like **11** and **12** (Chart 5) synthesized recently by Bertrand et al.[11] using the PMO theory. Even though the allene geometry is forced to be bent because the skeleton is built in the small four-membered and five-membered rings, the PMO theory should be applicable for the description of the electronic structure. The effects of introducing electron-donating substituents like nitrogen and oxygen at terminal allene carbons would be twofold. We may start the MO description from a similar MO diagram shown in Figure 8. In this MO diagram, the introduction of the electron-donating substituents elevates the ϕ_{a2} and ϕ_{b2} due to the interaction of these orbitals with lone-pair orbitals on the substituents and lowers the ξ_{a1} and ξ_{b1} due to the electron-withdrawing inductive effects of these substituents; the discussion is similar to the explanation of the enhanced singlet−triplet separation in the component carbene. The former effects remove the degeneracy of π_{a2} and π_{a1}, and the molecule would be singlet even at the D_{2h} geometry, where π_{a2} is vacant and π_{a1} should have the nature of lone-pair orbital. Lowering ξ_{a1} and ξ_{b1} gives relatively lower σ_{a1}* and σ_{b1}* through their interaction with χ_s and χ_x. In turn, lowering σ_{a1}* enhances the $\pi-\sigma^*$ mixing in these system. As the consequence of the orbital interaction, the HOMO−1, HOMO, and LUMO of these allenes should be π_{b2}, $\pi_{a1} + c\sigma_{a1}$*, and π_{a2}, respectively. The orbital sequence is in good accord with those for **12** calculated by a DFT method.[11b]

Recently, Frenking et al. have suggested[26] that the electronic configuration of a "trisilaallene" should be described as $R_2Si{:}\rightarrow Si\leftarrow{:}SiR_2$ by analogy with the electronic characteristics of $C(PR_3)_2$[35a] and $C(NHC)_2$[35b] (NHC = *N*-heterocyclic carbene). Apparently, their bonding description of trisilaallenes is not compatible with our above analysis describing the bonding as bent perpendicular allenic or zwitteionic. The Frenking's structure seems to be an extreme case of our bonding analysis using the PMO theory. The structure is obtained if low-lying pπ-type orbitals in R_2M---MR_2 fragments (ϕ_a and ϕ_b in Figure 5 and ϕ_{a2} and ϕ_{b2} in Figure 8) are absent as shown in Figure 10. Because this type of vacant orbitals is absent or high-lying in $C(PR_3)_2$ and $C(NHC)_2$, the Frenking's structure may be applicable to these molecules and heavy allenes may have the nature to some extent. However, neglecting the lowest vacant pπ orbital in heavy carbenes $:MR_2$ (R = H, alkyl, etc.) will not be rationalized because they show red-shifted $n\rightarrow$ pπ absorption bands,[13,14,36] give the corresponding radical anion by single-electron reduction using alkali metals,[37] and dimerize to the corresponding heavy ethylenes,[38] and π back-donation is significant in $(R_2Si)_2Pd$.[39]

Conclusion

Unusual bonding, structure, and properties of heavy allenes are summarized and comparatively discussed. Using the PMO theory, the origin of the bent and fluxional skeleton of heavy allenes is ascribed to the effective $\pi-\sigma^*$ distortion. The $\pi-\sigma^*$ distortion is caused by the existence of a σ^* orbital in heavy allenes which is relatively low-lying because of the hybridization defects in heavy main-group elements. The rather unusual structure of trisilaallenes proposed recently by Frenking et al.[26] is explained using the PMO theory as an extreme where the vacant pπ-type orbital of R_2Si: is high-lying and unavailable for bonding. The $\pi-\sigma^*$ distortion is a general useful model to understand qualitatively the bonding and structure of unsaturated compounds of heavy main-group elements. Several important issues including the reason for difference in the Si═Ge double bond distance between **1b** and **1c** and the origin of the remarkably reduced forbidden nature of the longest wavelength band in **1c** and **1d** will be related to the difference in the intrinsic nature between Si and Ge but still remain to be analyzed.

Acknowledgment. This work was supported by the Ministry of Education, Culture, Sports, Science, and Technology of Japan [Grant-in-Aids for Scientific Research on Priority Areas (No. 14078203, "Reaction Control of Dynamic Complexes", M.K.) and Specially Promoted Research (No. 17002005, M.K. and T.I.)].

Supporting Information Available: Experimental details for an alternative synthesis of **1d**, UV−vis spectra of **1a**−**1d**, details of the DFT calculations for energies and geometries of **1a′**−**1d′** at various geometries, and TD-DFT calculations of UV−vis spectra of **1a′**−**1d′**. This material is available free of charge via the Internet at http://pubs.acs.org.

JA904525A

(37) Ishida, S.; Iwamoto, T.; Kira, M. *J. Am. Chem. Soc.* **2003**, *125*, 3212.
(38) Silylene **2** and germylene **3** do not dimerize in reality. However, less sterically hindered silylenes and germylenes are known to dimerize to the corresponding heavy ethylenes.[1] See also: Tanaka, R.; Iwamoto, T.; Kira, M. *Angew. Chem., Int. Ed. Engl.* **2006**, *45*, 6371.
(39) Watanabe, C.; Iwamoto, T.; Kabuto, C.; Kira, M. *Angew. Chem., Int. Ed.* **2008**, *47*, 5386.